INT. J. NUM. METH. HEAT FLUID FLOW, VOL. 2, 455–467 (1992)

NATURAL CONVECTION IN A HORIZONTAL CONCENTRIC CYLINDRICAL ANNULUS

V. K. GARG* and A. Z. SZERI

Department of Mechanical Engineering, University of Pittsburgh, Pittsburgh, PA 15261, USA

ABSTRACT

This numerical study of natural convection flow in a horizontal cylindrical annulus is aimed at establishing the utility of the Galerkin–spline formulation for natural convection problems. The annulus has isothermal walls and the fluid is of constant material properties except for its density; density variation is incorporated via the Boussinesq approximation. Two formulations are employed, the velocity formulation and the streamfunction formulation. We are able to demonstrate the usefulness of the Galerkin–spline formulation for the problem and in comparison with published data, show that it leads to greater accuracy than the finite difference method. We also show the streamfunction formulation to be superior computationally to the velocity formulation. We find no bifurcation from the basic state up to 60,000 in Grashof number, even without *a priori* assumption of symmetry about the vertical plane. This last finding is in sharp contrast to results obtained when porous material fills the annulus.

KEY WORDS Natural convection Galerkin–spline formulation Cylindrical annulus

NOMENCLATURE

$A_i(r)$	normalized B-splines in the radial direction,
$b_j(\theta)$	normalized periodic B-splines in the tangential direction,
$B_j(\theta)$	normalized B-splines in the tangential direction,
C_l	coefficients in the expansion for cosine function,
DG	Jacobian of the system of equations,
g	acceleration due to gravity,
Gr	Grashof number based on the gap width,
k	order of the B-splines,
N	number of B-splines,
Nu	Nusselt number,
p	pressure,
Pr	Prandtl number of the fluid,
r	radial coordinate, dimensionless radial distance,
r_1, r_2	radii of inner and outer cylinders, respectively,
Ra	Rayleigh number based on the gap width $= GrPr$,
S_l	coefficients in the expansion for sine function,
T	temperature, dimensionless temperature $[=(T-T_2)/(T_1-T_2)]$,
T_1, T_2	temperature of the inner and outer cylinders, respectively,
t_{ij}	unknown coefficients in the expansion for T,

* Present address: NASA Lewis Research Center, Mail Stop 5-11, Cleveland, Ohio 44135, USA.

0961–5539/92/050455–13$2.00

Received February 1991
Revised November 1991

u dimensional, dimensionless radial velocity component,
u_{ij} unknown coefficients in the expansion for u,
v dimensional, dimensionless tangential velocity component,
v_{ij} unknown coefficients in the expansion for v,
x solution vector,
X dimensionless radial coordinate.

Greek

α thermal diffusivity of the fluid,
β coefficient of volumetric expansion of the fluid,
δ ratio of inner radius to gap width of the annulus,
ε relative error in global energy conservation,
η vector of state variables for the problem,
λ vector of parameters for the problem,
ν kinematic viscosity of the fluid,
θ tangential coordinate and the same divided by 2π,
σ step size in the parameter,
Ψ dimensionless stream function,
Ψ_{ij} unknown coefficients in the expansion for Ψ,
ω dimensional vorticity,
Ω dimensionless vorticity.

Subscripts

1 value at the inner cylinder,
2 value at the outer cylinder,
m mean value,
max maximum value,
r refers to radial direction,
θ refers to tangential direction.

Superscripts

k iteration counter,
T transpose of the matrix.

INTRODUCTION

Natural convection in enclosures is an important method of energy transfer which, for this reason, has received considerable attention in recent years. Applications of such flows include thermal storage systems, transmission cables, nuclear reactor design, cooling of electronic equipment, aircraft cabin insulation, etc. While an enclosure may be of any shape, the most studied one is the horizontal annulus of constant geometry. A review of earlier studies is available in Kuehn and Goldstein[1]. Various boundary conditions, including isothermal walls as well as fixed heat flux conditions on the walls have been studied[2–7]. Moreover, concentric and eccentric annuli with different diameter ratios have been investigated [8,9]. Effect of variable fluid properties on the heat transfer characteristics has also been researched by several authors[10,11]. To date, however, there are only a few solutions for free convective flow in a horizontal annulus *without* assuming flow symmetry about the vertical diameter.

We investigate this flow, with no *a priori* assumption of symmetry. Our conclusions are negative, however, in this respect: we find that the flow remains symmetric with respect to the vertical plane through the axis of the annulus for all the conditions tested. Although in thin annuli at either top or bottom locally the conditions superficially correspond to those of the Bernard problem, we find no bifurcation from the basic state. This finding is in stark contrast to the results of Himasekhar and Bau[12], who calculated flow in annuli containing saturated porous media, and found bifurcation.

The numerical strategy employed in this paper is projection of the governing equations onto a polynomial subspace with a B-spline basis. The resulting non-linear algebraic system is solved with parametric continuation in the Grashof number, using QR decomposition and Newton's method. We compare results from two formulations. Although the streamfunction formulation converges faster than the formulation based on the primitive variables, both formulations yield results superior in accuracy to those from the finite difference method. We show this by comparison with published finite difference data[1].

ANALYSIS

We consider here two horizontal co-axial cylinders of infinite lengths and of radii r_1 and r_2, $r_2 > r_1$, and write the relevant equations, employing the Boussinesq approximation for density variation, in cylindrical polar coordinates. The problem is modelled by four coupled partial differential equations: two momentum equations, in the r and the θ direction, respectively, the equation of mass conservation and the equation of energy. The two momentum equations contain derivatives of the pressure.

The real difficulty in the calculation of the velocity field lies in the unknown pressure field. The pressure field is only indirectly specified via the continuity equation; when the correct pressure field is substituted into the momentum equations, the resulting velocity field satisfies the continuity equation. Furthermore the only condition that may be specified on the pressure in an incompressible fluid is that $p=0$ at some point on the boundary. This indirect specification is not very useful for our purpose. To deal with this problem we eliminate the pressure by cross-differentiation between the equations of momentum. This manipulation yields the following mathematical model for natural convective flow in a cylindrical annulus:

$$-Xu\frac{\partial^2 v}{\partial r^2}+\frac{u}{2\pi}\frac{\partial^2 u}{\partial r\,\partial\theta}-\frac{v}{2\pi}\frac{\partial^2 v}{\partial r\,\partial\theta}+\frac{v}{4\pi^2 X}\frac{\partial^2 u}{\partial\theta^2}-\frac{u}{2\pi X}\frac{\partial u}{\partial\theta}-\frac{v}{\pi X}\frac{\partial v}{\partial\theta}-\frac{\partial}{\partial r}(uv)$$

$$=-Gr\left[X\cos(2\pi\theta)\frac{\partial T}{\partial r}-\frac{\sin(2\pi\theta)}{2\pi}\frac{\partial T}{\partial\theta}\right]+\frac{1}{8X^2\pi^3}\frac{\partial^3 u}{\partial\theta^3}-X\frac{\partial^3 v}{\partial r^3}+\frac{1}{2\pi}\frac{\partial^3 u}{\partial r^2\,\partial\theta}+$$

$$\frac{1}{X}\frac{\partial v}{\partial r}-\frac{v}{X^2}-\frac{1}{4\pi^2 X}\frac{\partial^3 v}{\partial r\,\partial\theta^2}-\frac{1}{4\pi^2 X^2}\frac{\partial^2 v}{\partial\theta^2}-2\frac{\partial^2 v}{\partial r^2}-\frac{1}{2\pi X}\frac{\partial^2 u}{\partial r\,\partial\theta}+\frac{1}{2\pi X^2}\frac{\partial u}{\partial\theta} \quad (1)$$

$$\frac{\partial u}{\partial r}+\frac{u}{X}+\frac{1}{2\pi X}\frac{\partial v}{\partial\theta}=0 \quad (2)$$

$$u\frac{\partial T}{\partial r}+\frac{v}{2\pi X}\frac{\partial T}{\partial\theta}=\frac{1}{Pr}\left[\frac{\partial^2 T}{\partial r^2}+\frac{1}{X}\frac{\partial T}{\partial r}+\frac{1}{(2\pi X)^2}\frac{\partial^2 T}{\partial\theta^2}\right] \quad (3)$$

where θ is measured anti-clockwise from the east position. The Grashof number, Gr, and the Prandtl number, Pr, have the definition:

$$Gr=\frac{g\beta(T_1-T_2)(r_2-r_1)^3}{\nu^2}, \qquad Pr=\frac{\nu}{\alpha}$$

Also we have used the non-dimensionalization

$$0 \leqslant \bar{r} = \frac{r - r_1}{r_2 - r_1} \leqslant 1, \qquad 0 \leqslant \bar{\theta} = \frac{\theta}{2\pi} \leqslant 1, \qquad X = \bar{r} + \delta, \qquad \delta = \frac{r_1}{r_2 - r_1}$$

$$\bar{u} = \frac{u(r_2 - r_1)}{\nu}, \qquad \bar{v} = \frac{v(r_2 - r_1)}{\nu}, \qquad \bar{T} = \frac{T - T_2}{T_1 - T_2}, \tag{4}$$

but dropped the overscore bar for convenience. Note that we make no assumption of symmetry.

We employ two representations in the calculations: (i) the velocity formulation, (1)–(3), and (ii) the streamfunction formulation, obtained by substituting into (1) and (3) for velocity components in terms of the streamfunction.

Velocity formulation

The equations pertinent here are (1), (2) and (3). The velocity boundary conditions are no slip at the walls. Since we are dealing with incompressible fluids, we may also set the condition that p=constant, say, at the point $(r, \theta) = (0, 0)$. When eliminating the pressure, we increased the order of the momentum equations. To assure smooth solution, we evaluate the equation of continuity at the walls $r = 0$, 1 and obtain the regularity condition of zero normal derivative of axial velocity at the walls[13]. The boundary conditions, therefore, are:

$$u = 0, \qquad v = 0, \qquad \frac{\partial u}{\partial r} = 0, \qquad T = 1 \qquad \text{at} \quad r = 0$$

$$u = 0, \qquad v = 0, \qquad \frac{\partial u}{\partial r} = 0, \qquad T = 0 \qquad \text{at} \quad r = 1 \tag{5}$$

We intend to approximate $\{u(r, \theta), v(r, \theta), T(r, \theta)\}$, which is given only implicitly as solution of (1), (2), (3) and (5), by piecewise polynomial functions. Thus we partition the interval [0, 1] as:

$$\pi\colon 0 = r_1 < r_2 < \cdots < r_l < r_{l+1} = 1$$

and let t: $\{t_j\}^{N+k}$ be the non-decreasing knot sequence such that:

$$N = k + l - 1$$

$$t_i = r_1, \qquad i = 1, \ldots, k$$

$$t_i = r_{i-k+1}, \qquad i = k+1, \ldots, k+l-1$$

$$t_i = r_{l+1}, \qquad i = k+l, \ldots, k+N \tag{6}$$

Construct a sequence $A_1, \ldots, A_N$ of B-splines of order k for the knot sequence t by the recurrence relation[14]

$$A_{i,k}(r) = \frac{r - t_i}{t_{i+k-1} - t_i} A_{i,k-1}(r) + \frac{t_{i+k} - r}{t_{i+k} - t_{i+k+1}}(r), \qquad i = 1, 2, 3, \ldots, N$$

$$A_{j,1}(r) = \begin{cases} 1 & \text{for } r \in [t_j, t_{j+1}] \\ 0 & \text{otherwise} \end{cases} \tag{7}$$

According to the Curry–Schoenberg theorem[14], the sequence $\{A_j\}$ forms a basis for the kth order piecewise polynomial space with breakpoint sequence π and $k-2$ continuous derivatives at internal breakpoints. In symbols we can write

$$\mathscr{P}_{k,\pi} = \left\{ \sum_{i=1}^{N} \alpha_i A_i(r);\ \alpha_i \text{ real for all } i \right\}$$

The B-splines thus defined provide a partition of unity:

$$\left.\begin{array}{l} A_i(r)\geqslant 0, \quad 1\leqslant i\leqslant N \\ \sum_{i=1}^{N} A_i(r)=1 \end{array}\right\} r\in[r_1, r_{l+1}]$$

In the present calculations we employ various values of k, the order of splines in the basis. Let $\{A_i(r): 1\leqslant i\leqslant N_r\}$ be the set of normalized B-splines relative to k_r, π_r and let $\{B_j(\theta): 1\leqslant j\leqslant N_\theta\}$ be the set of normalized B-splines relative to k_θ, π_θ.

To assure that the solution is periodic in θ, we require that:

$$\left.\frac{\partial^n \Pi(r,\theta)}{\partial\theta^n}\right|_{\theta=0}=\left.\frac{\partial^n \Pi(r,\theta)}{\partial\theta^n}\right|_{\theta=1} \qquad \Pi=u,v,T \qquad n\geqslant 0, r\in[0,1] \tag{8}$$

The simplest way to assure satisfaction of (8) is by re-definition of the spline basis. Let $c=-2B_2''(0)/B_3''(0)$ and define the matrices Φ and Σ and the vector b:

$$\Phi=\begin{bmatrix} I_3 & 0 & \Sigma \\ 0 & I_{N_\theta-6} & 0 \end{bmatrix}, \qquad \Sigma=\begin{bmatrix} c & 2 & 1 \\ -c & -1 & 0 \\ 1 & 0 & 0 \end{bmatrix}$$

$$b=\Phi B=(b_1,\ldots,b_{N_\theta-3})^{\mathrm{T}} \qquad B=(B_1,\ldots,B_{N_\theta})^{\mathrm{T}} \tag{9}$$

It can be verified that the sequence $\{b_i(\theta),\ 1\leqslant i\leqslant N_\theta-3\}$ is a basis for the subspace of $\mathscr{P}_{k,\pi}$ defined as:

$$S_{k,\pi}=\{s(r)\in\mathscr{P}_{k,\pi};\ s^{(l)}(0)=s^{(l)}(1),\ l=0,1,2\}$$

Denote the usual B-spline basis in r by A, the periodic B-spline basis in θ by b, then the basis for approximating $\{u(r,\theta),\ v(r,\theta),\ T(r,\theta)\}$ is $A\otimes b$ and the expansions:

$$u(r,\theta)=\sum_{i=3}^{N_r-2}\sum_{j=1}^{N_\theta-3} u_{ij}A_i(r)b_j(\theta)$$

$$v(r,\theta)=\sum_{i=2}^{N_r-1}\sum_{j=1}^{N_\theta-3} v_{ij}A_i(r)b_j(\theta)$$

$$T(r,\theta)=\sum_{i=2}^{N_r-1}\sum_{j=1}^{N_\theta-3} t_{ij}A_i(r)b_j(\theta)+\sum_{i=1}^{N_r-1} A_i(r) \tag{10}$$

satisfy the boundary condition (5) as well as the periodicity conditions (8) of the problem.

With the expansions in (10), the continuity, momentum and energy equations (1), (2) and (3) discretize to:

$$\sum_{i=3}^{N_r-2}\sum_{j=1}^{N_\theta-3} u_{ij}\bar{z}_{lj}^{(0)}(\overline{\mathbf{p1}}_{ki}^{(1)}+\overline{\mathbf{p0}}_{ki}^{(0)})+\frac{1}{2\pi}\sum_{i=2}^{N_r-1}\sum_{j=1}^{N_\theta-3} v_{ij}\overline{\mathbf{p0}}_{ki}^{(0)}\bar{z}_{lj}^{(1)}=0$$

$$(3\leqslant k\leqslant N_r-2;\ 1\leqslant l\leqslant N_\theta-3) \tag{11}$$

$$\frac{1}{2\pi}\sum_{i=3}^{N_r-2}\sum_{j=1}^{N_\theta-3} u_{ij}\left[\bar{z}_{jl}^{(1)}(\overline{\mathbf{p1}}_{ki}^{(3)}+\overline{\mathbf{n1}}_{ki}^{(0)})-\frac{1}{4\pi^2}\overline{\mathbf{n1}}_{ki}^{(0)}\bar{z}_{lj}^{(4)}+2\bar{z}_{lj}^{(1)}(\overline{\mathbf{p0}}_{ik}^{(1)}+\overline{\mathbf{n1}}_{ki}^{(0)})\right]+$$

$$\sum_{i=2}^{N_r-1}\sum_{j=1}^{N_\theta-3} v_{ij}\left[\bar{z}_{lj}^{(0)}(-\overline{\mathbf{n1}}_{ki}^{(0)}+\overline{\mathbf{p2}}_{ki}^{(4)}-\overline{\mathbf{p0}}_{ik}^{(1)})-\frac{1}{4\pi^2}\bar{z}_{lj}^{(3)}(\overline{\mathbf{n1}}_{ki}^{(0)}+\overline{\mathbf{p0}}_{ik}^{(0)})+\frac{1}{2\pi^2}\bar{z}_{jl}^{(3)}\overline{\mathbf{n1}}_{ki}^{(0)}\right]-$$

$$\sum_{i=3}^{N_r-2}\sum_{j=1}^{N_\theta-3}\sum_{m=2}^{N_r-1}\sum_{n=1}^{N_\theta-3} u_{ij}v_{mn}\bar{\mathbf{Z}}^{(0)}_{ljn}(\overline{\mathbf{P0}}^{(0)}_{kim}+\overline{\mathbf{P1}}^{(1)}_{imk}+\overline{\mathbf{P1}}^{(1)}_{kim}+\overline{\mathbf{P2}}^{(3)}_{ikm})+$$
$$\frac{1}{2\pi}\sum_{i=3}^{N_r-2}\sum_{j=1}^{N_\theta-3}\sum_{m=3}^{N_r-2}\sum_{n=1}^{N_\theta-3} u_{ij}u_{mn}\bar{\mathbf{Z}}^{(1)}_{jnl}\overline{\mathbf{P1}}^{(1)}_{kim}-$$
$$\frac{1}{2\pi}\sum_{i=2}^{N_r-1}\sum_{j=1}^{N_\theta-3}\sum_{m=2}^{N_r-1}\sum_{n=1}^{N_\theta-3} v_{ij}v_{mn}[\bar{\mathbf{Z}}^{(1)}_{ljn}(\overline{\mathbf{P0}}^{(0)}_{kim}+\overline{\mathbf{P1}}^{(1)}_{imk})+\bar{\mathbf{Z}}^{(1)}_{jnl}\overline{\mathbf{P0}}^{(0)}_{kim}]+$$
$$\frac{1}{4\pi^2}\sum_{i=2}^{N_r-1}\sum_{j=1}^{N_\theta-3}\sum_{m=3}^{N_r-2}\sum_{n=1}^{N_\theta-3} v_{ij}u_{mn}\overline{\mathbf{P0}}^{(0)}_{kim}\bar{\mathbf{Z}}^{(3)}_{jnl}-Gr\sum_{i=2}^{N_r-1}\sum_{j=1}^{N_\theta-3}\sum_{m=1}^{N_\theta-3} C_m t_{ij}\overline{\mathbf{p2}}^{(1)}_{ki}\bar{\mathbf{Z}}^{(0)}_{ljm}-$$
$$Gr\sum_{i=1}^{N_r-1}\sum_{m=1}^{N_\theta-3} C_m\overline{\mathbf{p2}}^{(1)}_{ki}\bar{\mathbf{z}}^{(0)}_{lm}+\frac{Gr}{2\pi}\sum_{i=2}^{N_r-1}\sum_{j=1}^{N_\theta-3}\sum_{m=1}^{N_\theta-3} S_m t_{ij}\overline{\mathbf{p1}}^{(0)}_{ki}\bar{\mathbf{Z}}^{(1)}_{lmj}=0$$
$$(2\leqslant k\leqslant N_r-1,\ 1\leqslant l\leqslant N_\theta-3) \tag{12}$$

$$Pr\sum_{i=2}^{N_r-1}\sum_{j=1}^{N_\theta-3}\sum_{m=3}^{N_r-2}\sum_{n=1}^{N_\theta-3} u_{mn}t_{ij}\overline{\mathbf{P1}}^{(1)}_{kmi}\bar{\mathbf{Z}}^{(0)}_{lnj}+Pr\sum_{i=1}^{N_r-1}\sum_{m=3}^{N_r-2}\sum_{n=1}^{N_\theta-3} u_{mn}\overline{\mathbf{P1}}^{(1)}_{kmi}\bar{\mathbf{z}}^{(0)}_{ln}+$$
$$\frac{Pr}{2\pi}\sum_{i=2}^{N_r-1}\sum_{j=1}^{N_\theta-3}\sum_{m=2}^{N_r-1}\sum_{n=1}^{N_\theta-3} v_{mn}t_{ij}\overline{\mathbf{P0}}^{(0)}_{kmi}\bar{\mathbf{Z}}^{(1)}_{lnj}+\sum_{i=1}^{N_r-1}\bar{\mathbf{b}}^{(0)}_{l}\overline{\mathbf{p1}}^{(3)}_{ki}+$$
$$\sum_{i=2}^{N_r-1}\sum_{j=1}^{N_\theta-3} t_{ij}\left[\bar{\mathbf{z}}^{(0)}_{lj}\overline{\mathbf{p1}}^{(3)}_{ki}+\frac{1}{4\pi^2}\overline{\mathbf{n1}}^{(0)}_{ki}\bar{\mathbf{z}}^{(3)}_{lj}\right]=0$$
$$(2\leqslant k\leqslant N_r-1;\ 1\leqslant l\leqslant N_\theta-3) \tag{13}$$

Here C_j and S_j are the coefficients in the expansions for cos and sin functions, respectively, as follows

$$\cos(2\pi\theta)=\sum_{j=1}^{N_\theta-3} C_j b_j(\theta)$$
$$\sin(2\pi\theta)=\sum_{j=1}^{N_\theta-3} S_j b_j(\theta) \tag{14}$$

The Galerkin coefficients $\bar{\mathbf{z}}^{(0)}_{lj}$, $\overline{\mathbf{p0}}^{(2)}_{ki}$,... are defined in the Appendix.

Streamfunction formulation

We can easily eliminate the equation of continuity (2) from further consideration if the dimensionless streamfunction $\Psi(r,\theta)$ is used to represent the velocity field:

$$u=\frac{1}{X}\frac{\partial\Psi}{\partial\theta},\qquad v=-2\pi\frac{\partial\Psi}{\partial r} \tag{15}$$

In terms of Ψ the kinematic boundary conditions are:

$$\Psi=\frac{\partial\Psi}{\partial r}=0\quad\text{at}\quad r=0,1 \tag{16}$$

where we postulate zero net circulation.

The streamfunction $\Psi(r,\theta)$ and the temperature $T(r,\theta)$ are assumed to have the representation:

$$\Psi(r,\theta)=\sum_{i=3}^{N_r-2}\sum_{j=1}^{N_\theta-3}\Psi_{ij}A_i(r)b_j(\theta)$$

$$T(r,\theta)=\sum_{i=2}^{N_r-1}\sum_{j=1}^{N_\theta-3}t_{ij}A_i(r)b_j(\theta)+\sum_{i=1}^{N_r-1}A_i(r) \tag{17}$$

These expansions satisfy both boundary and periodicity conditions.

With definition (15) and expansion (17) substituted into (1) and (3), application of Galerkin's procedure leads to the following two sets of equations:

$$\sum_{i=3}^{N_r-2}\sum_{j=1}^{N_\theta-3}\Psi_{ij}\Bigg\{\sum_{k=3}^{N_r-2}\sum_{l=1}^{N_\theta-3}\Psi_{kl}\Bigg[-2\pi Z_{nlj}^{(1)}(\overline{\mathbf{P1}}_{mik}^{(4)}+\overline{\mathbf{P1}}_{imk}^{(4)}+\overline{\mathbf{N1}}_{mik}^{(1)})-\frac{1}{\pi}\overline{\mathbf{N2}}_{mki}^{(0)}\bar{\mathbf{Z}}_{njl}^{(4)}+$$
$$\frac{1}{2\pi}\overline{\mathbf{N1}}_{mik}^{(1)}\bar{\mathbf{Z}}_{njl}^{(4)}-2\pi\overline{\mathbf{P1}}_{mik}^{(4)}\bar{\mathbf{Z}}_{njl}^{(1)}+\frac{1}{2\pi}\overline{\mathbf{N1}}_{mki}^{(1)}(\bar{\mathbf{Z}}_{njl}^{(4)}+\bar{\mathbf{Z}}_{jnl}^{(4)})-2\pi\overline{\mathbf{P0}}_{mki}^{(3)}\bar{\mathbf{Z}}_{njl}^{(1)}\Bigg]-$$
$$\frac{1}{8\pi^3}\overline{\mathbf{n2}}_{mi}^{(0)}\bar{\mathbf{z}}_{nj}^{(5)}-2\pi\bar{\mathbf{z}}_{nj}^{(0)}[\overline{\mathbf{p0}}_{mi}^{(3)}+2\overline{\mathbf{p1}}_{mi}^{(4)}+\overline{\mathbf{p2}}_{mi}^{(5)}+\overline{\mathbf{n1}}_{mi}^{(1)}]+\frac{1}{\pi}\bar{\mathbf{z}}_{nj}^{(3)}[2\overline{\mathbf{n2}}_{mi}^{(0)}-\overline{\mathbf{n1}}_{mi}^{(1)}-\overline{\mathbf{p0}}_{mi}^{(3)}]\Bigg\}+$$
$$Gr\sum_{i=1}^{N_r-1}\overline{\mathbf{p2}}_{mi}^{(1)}\overline{\mathbf{bc}}_{n}^{(0)}+Gr\sum_{i=2}^{N_r-1}\sum_{j=1}^{N_\theta-3}t_{ij}\Bigg[\overline{\mathbf{p2}}_{mi}^{(1)}\overline{\mathbf{zc}}_{nj}^{(0)}-\frac{1}{2\pi}\overline{\mathbf{p1}}_{mi}^{(0)}\overline{\mathbf{zs}}_{nj}^{(1)}\Bigg]=0$$
$$(3\leqslant m\leqslant N_r-2;\ 1\leqslant n\leqslant N_\theta-3) \tag{18}$$

$$\sum_{i=2}^{N_r-1}\sum_{j=1}^{N_\theta-3}t_{ij}\Bigg\{Pr\sum_{k=3}^{N_r-2}\sum_{l=1}^{N_\theta-3}\Psi_{kl}(-\bar{\mathbf{Z}}_{nlj}^{(1)}\overline{\mathbf{P0}}_{mik}^{(1)}+\bar{\mathbf{Z}}_{njl}^{(1)}\overline{\mathbf{P0}}_{mki}^{(1)})+\bar{\mathbf{z}}_{nj}^{(0)}\overline{\mathbf{p1}}_{mi}^{(3)}+\frac{1}{4\pi^2}\overline{\mathbf{n1}}_{mi}^{(0)}\bar{\mathbf{z}}_{nj}^{(3)}\Bigg\}+$$
$$\sum_{S=1}^{N_r-1}\Bigg\{\bar{\mathbf{b}}_{n}^{(0)}\overline{\mathbf{p1}}_{mS}^{(3)}+Pr\sum_{i=3}^{N_r-2}\sum_{j=1}^{N_\theta-3}\Psi_{ij}\overline{\mathbf{P0}}_{miS}^{(1)}\bar{\mathbf{z}}_{nj}^{(1)}\Bigg\}=0$$
$$(2\leqslant m\leqslant N_r-1;\ 1\leqslant n\leqslant N_\theta-3) \tag{19}$$

Continuation of the solution

The discretized equations, (11)–(13) or (18), (19) can be written in the form:

$$G(\eta,\lambda)=0 \tag{20}$$

where G: $R^n=H\oplus\Lambda\to R^m$ is a C^l-mapping ($l>2$), dim $H=m$ and dim $\Lambda=n-m>1$. Here $\eta\in H$ is a vector of state variables, $\{u_{ij},v_{ij},t_{ij}\}$ or $\{\Psi_{ij},t_{ij}\}$, and $\lambda\in\Lambda$ is a vector of parameters Gr,Pr,δ.

In the computational scheme we fix two of the parameters, say Pr and δ, and vary the Grashof number Gr; thus $n-m=1$ and the regular manifold of (20) is a path.

Local iteration. We use the Gauss–Newton method for local iteration[15]. Denoting (η,λ) by x for convenience, the iteration sequence is defined by:

$$x^{k+1}=x^k-[DG(x^k)^{\mathrm{T}}DG(x^k)]^{-1}DG(x^k)^{\mathrm{T}}G(x^k) \tag{21}$$

where $DG(x^k)$ is the Jacobian of G evaluated at x^k.

Equation (21) is computationally inconvenient. It can be verified, however, that x^{k+1} will satisfy (21) if it satisfies the condition:

$$DG(x^k)(x^k-x^{k+1})=G(x^k) \tag{22}$$

Numerically (22) can be implemented in various ways. With $Q\mathscr{R}$ factorization of $DG(x^k)^T$,

$$DG(x^k)^T = Q\begin{pmatrix}\mathscr{R}\\ 0\end{pmatrix} \tag{23}$$

where $Q \in R^{n\times n}$ is orthogonal and $\mathscr{R} \in \mathscr{R}^{m\times m}$ is upper triangular. This implies that

$$x^k - x^{k+1} = Q\begin{pmatrix}\mathscr{R}^{-T}\\ 0\end{pmatrix}G(x^k) \tag{24}$$

is a solution of (22).

The Gauss–Newton method can now be represented by the algorithm:

(i) set $x^\circ = x$;
(ii) for $k = 0, 1, \ldots$ until convergence
  (a) solve the triangular system $\mathscr{R}^T y = G(x^k)$ for $y \in R^n$;
  (b) compute the next iterate $x^{k+1} = x^k - Q\begin{pmatrix}y\\ 0\end{pmatrix}$

Continuation along the path. For a solution point x on the path, again, we consider the $Q\mathscr{R}$ factorization $DG(x)^T$

$$DG(x)^T = Q\begin{pmatrix}\mathscr{R}\\ 0\end{pmatrix}$$

Clearly the last column vector of the orthogonal matrix Q, namely Qe_n, is the tangent vector of the path. Here $e_n = (0, \ldots, 0, 1)^T \in R^n$ at x.

The simplest way to get a predictor x° for the next point on the path is to set

$$x^\circ = x + \sigma Q e_n \tag{25}$$

where σ is a suitable step size.

When the λ-component of the tangent Qe_n equals zero, the tangent vector is orthogonal to Λ. This is a necessary condition for a turning point. A bifurcation point x^* on the path, on the other hand, is characterized by rank $(DG(x^*)) < n$. There are also conditions on the second derivative. For technical details the reader is referred to Joseph[16] and Keller[17].

RESULTS AND DISCUSSION

We have employed the Galerkin–spline formulation in the past for recirculating flows[18–20], for swirling flows of non-Newtonian fluids[21,22], for linear stability calculations[23] and for path

Table 1 Relative error in global energy conservation ($Pr = 0.7$, $r_2/r_1 = 2.6$, $k_r = k_\theta = 5$)

	Ra		
$N_r = N_\theta$	1000	10,000	50,000
11	0.00091	0.00716	0.0464
15	0.00011	0.00456	0.0064
19	0.00003	0.00134	0.0045
23	0.00001	0.00034	0.0059
27	0.00000	0.00008	0.0045
31	0.00000	0.00001	0.0031
FD method[1]	0.0028	0.0025	0.0170

continuation and bifurcation analysis[24], always with good results. Here we investigate the utility of the Galerkin–spline formulation for natural convection problems, and its accuracy relative to the finite difference method in such problems. This constitutes our first objective for the present paper. The second objective is a comparison, from a computational point of view, between two formulations: (1) the velocity formulation and (2) the streamfunction formulation.

We will examine the suitability of the Galerkin–spline formulation for our natural convection problem and its accuracy via the streamfunction formulation. The accuracy of the formulation depends on two parameters, the number of splines, N_r, N_θ, in expansion (17) and the order k_r, k_θ, of the splines in the expansion. For simplicity we set $N_r=N_\theta=N$ and $k_r=k_\theta=k$ in the sequel. Satisfaction of global energy balance can be estimated by comparing average values of the Nusselt number Nu_1 and Nu_2, calculated on the inner and outer cylinders, respectively. We define a relative error ε for global energy conservation by:

$$\varepsilon=\frac{2|Nu_1-Nu_2|}{(Nu_1+Nu_2)}$$

For the conditions $Pr=0.7$ and $r_2/r_1=2.6$ we obtained ε values as shown in *Table 1*. The entries of this table were calculated with $k=5$ and various number of terms in the expansion (17). This Table also contains values obtained from the finite difference result of Kuehn and Goldstein[1]. We use the Rayleigh number, $Ra=Pr\,Gr$, in this comparison. Convergence in ε is monotonic for small values of the Rayleigh number.

The effect of varying N_r, N_θ is shown in *Table 2* in another way by displaying the mean Nusselt number $(Nu)_m=(Nu_1+Nu_2)/2$. Convergence, which is monotonic, seems to be considerably faster when $k_r=k_\theta$ is increased from 4 to 5.

The effect of varying the order of splines k_r, k_θ is demonstrated in *Table 3*. Even at $Ra=50{,}000$ changing $k_r=k_\theta$ from 5 to 6 changes $(Nu)_m$ only by 1 in 3000, showing rapid convergence with order of splines.

In *Table 4* we compare the two formulations, calculating $(Nu)_m$ from the low order system $N_r=N_\theta=11$ and $k_r=k_\theta=4$. The 'error' displayed here was calculated relative to the solution obtained with $N_r=N_\theta=20$ and $k_r=k_\theta=5$ using the streamfunction formulation. The latter solutions can be shown to have converged to better than 1 in 1000. The streamfunction

Table 2 Mean Nusselt number ($Pr=0.7$, $r_2/r_1=2.6$, $Ra=50{,}000$)

	$N_r=N_\theta$			
$k_r=k_\theta$	11	15	19	23
4		3.0277		3.0834
5	2.9461	3.0540	3.0954	3.1025

Table 3 Mean Nusselt number ($Pr=0.7$, $r_2/r_1=2.6$, $N_r=N_\theta=23$)

	$k_r=k_\theta$		
Ra	4	5	6
30,000	2.7422	2.7504	2.7491
50,000	3.0834	3.1025	3.1034

Table 4 Mean Nusselt number ($Pr=0.7$, $r_2/r_1=2.6$, $N_r=N_\theta=11$, $k_r=k_\theta=4$)

	Gr		
Formulation	3000	6000	10,000
Velocity	1.3915	1.6890	2.5145
(error)	(0.072)	(0.074)	(0.640)
Streamfunction	1.4120	1.7045	1.9525
(error)	(0.092)	(0.090)	(0.078)

formulation can be seen to be significantly better than the velocity formulation at high Grashof numbers, considering the 'error' in *Table 4* and the fact that $N_r = N_\theta = 11$ yields a system of 128 equations in the streamfunction formulation but a system of 200 equations in the velocity formulation.

Table 5 contains a comparison of local and average Nusselt numbers from our stream function formulation with $k_r = k_\theta = 5$ at $Pr = 0.7$ and $r_2/r_1 = 2.6$, with data from finite difference calculations[1] at three Rayleigh numbers. These results show significant differences between the two sets of data, up to 18% at $Ra = 50{,}000$.

Having established the accuracy of the present method, we present some results in *Figures 1–3*. *Figure 1* shows the temperature profiles at $Ra = 50{,}000$, $Pr = 0.7$, and $r_2/r_1 = 2.6$ for various angular locations measured clockwise from the north position. These profiles match very well with those in Figure 15 of Kuehn and Goldstein[1], and are presented for many more angular locations than those in Kuehn and Goldstein[1]. The temperature profiles clearly show the radial temperature inversion indicating the separation of inner- and outer-cylinder thermal boundary layers. Thus the fluid near the cool outer cylinder is warmer than that closer to the hot inner

Table 5 Comparison of local and average Nusselt numbers ($Pr = 0.7$, $r_2/r_1 = 2.6$, $k = 5$)

			Nusselt number							
Ra	Location	*N*	0°	30°	60°	90°	120°	150°	180°	Avg.
1,000	inner	11	0.606	0.713	0.947	1.191	1.379	1.492	1.529	1.132
		15	0.606	0.713	0.947	1.191	1.381	1.494	1.531	1.132
		19	0.606	0.713	0.947	1.192	1.381	1.494	1.532	1.132
		23	0.606	0.713	0.947	1.192	1.381	1.494	1.532	1.133
Kuehn & Goldstein[1]			0.57	0.67	0.90	1.14	1.32	1.44	1.47	1.081
	outer	11	1.847	1.707	1.384	1.043	0.789	0.647	0.602	1.133
		15	1.846	1.707	1.384	1.043	0.789	0.647	0.602	1.133
		19	1.846	1.707	1.384	1.043	0.789	0.647	0.602	1.133
		23	1.846	1.707	1.384	1.043	0.789	0.647	0.602	1.133
Kuehn & Goldstein[1]			1.78	1.64	1.33	1.00	0.75	0.61	0.57	1.084
10,000	inner	11	0.401	0.961	1.729	2.388	2.721	2.823	2.886	2.046
		15	0.409	0.968	1.746	2.420	2.747	2.858	2.904	2.067
		19	0.415	0.967	1.745	2.423	2.752	2.864	2.909	2.070
		23	0.417	0.966	1.744	2.423	2.753	2.865	2.911	2.071
Kuehn & Goldstein[1]			0.37	0.90	1.64	2.33	2.70	2.85	2.90	2.010
	outer	11	5.325	4.198	2.803	1.624	0.729	0.279	0.160	2.061
		15	5.527	4.201	2.798	1.621	0.730	0.281	0.165	2.076
		19	5.485	4.196	2.798	1.622	0.730	0.281	0.165	2.073
		23	5.458	4.194	2.798	1.622	0.730	0.281	0.165	2.071
Kuehn & Goldstein[1]			5.35	4.10	2.72	1.54	0.68	0.26	0.14	2.005
50,000	inner	11	0.717	1.816	2.708	3.356	3.915	4.082	3.611	3.014
		15	0.619	1.880	2.744	3.383	4.056	3.982	3.931	3.064
		19	0.642	1.880	2.754	3.410	4.095	4.022	4.011	3.089
		23	0.646	1.879	2.756	3.416	4.104	4.033	4.016	3.093
Kuehn & Goldstein[1]			0.53	1.68	2.58	3.28	3.97	4.15	4.32	3.024
	outer	11	8.316	5.490	3.468	2.451	1.361	0.291	0.154	2.878
		15	10.216	5.572	3.496	2.464	1.340	0.288	0.135	3.044
		19	10.933	5.623	3.514	2.474	1.345	0.288	0.141	3.102
		23	11.094	5.623	3.516	2.474	1.345	0.289	0.141	3.112
Kuehn & Goldstein[1]			10.77	5.57	3.45	2.28	1.10	0.26	0.12	2.973

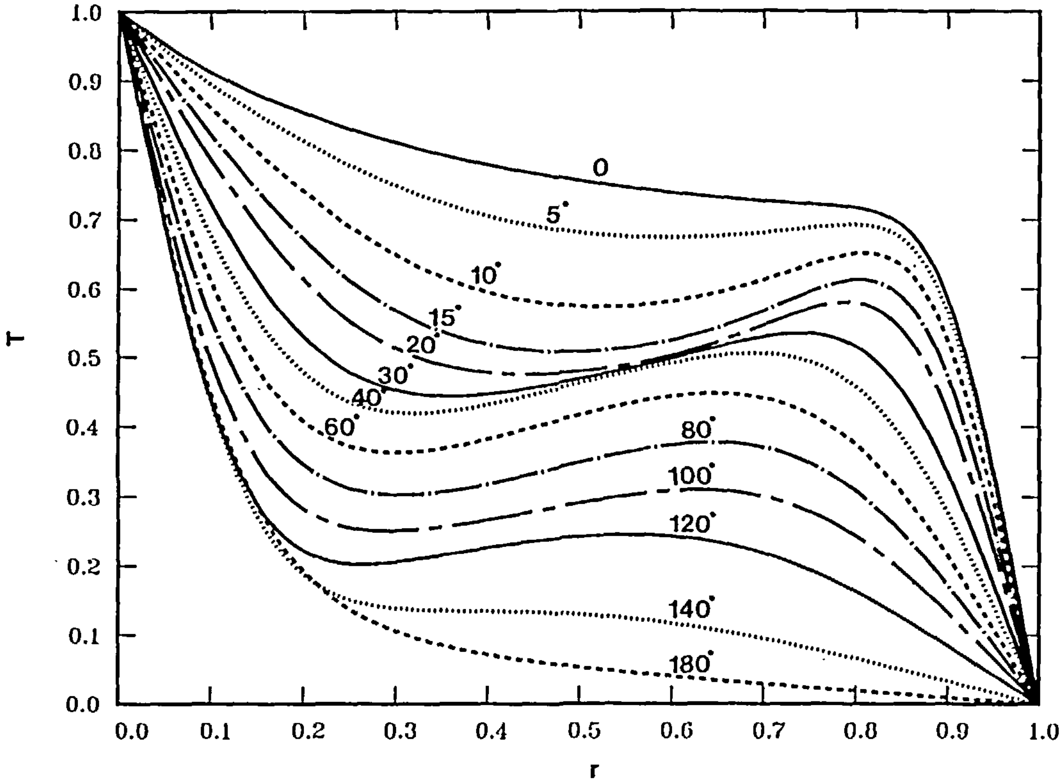

Figure 1 Temperature profiles for $Ra=50{,}000$, $Pr=0.7$ and $r_2/r_1=2.6$ at various angular locations measured from the north position,——, $\theta=0, 30°, 120°$; ···, $\theta=5°, 40°, 140°$; – – –, $\theta=10°, 60°, 180°$; —·—, $\theta=15°, 80°$; — — —, $\theta=20°, 100°$

cylinder. This phenomenon has also been observed in natural convection between concentric spheres[25] and in a vertical slot[26]. Heat is convected from the lower portion of the inner cylinder to the top of the outer cylinder.

As shown in *Figure 2*, vorticity in the central core is almost constant near this Rayleigh number, indicating a region approaching solid-body rotation, and similar to flow in a vertical slot[27]. The dimensionless vorticity, Ω, plotted in *Figures 2* and *3*, is defined as:

$$\Omega=\frac{\omega(r_2-r_1)^2}{2\pi\nu}=-\frac{\partial^2\Psi}{\partial r^2}-\frac{1}{X}\frac{\partial\Psi}{\partial r}-\frac{1}{4\pi^2X^2}\frac{\partial^2\Psi}{\partial\theta^2} \tag{26}$$

where ω is the dimensional vorticity. We may note that with Ψ known in terms of an expansion in B-splines, it is relatively easy to find Ω from (26). *Figures 2* and *3* show the Ω values normalized by $|\Omega|_{max}$ at various angular locations measured clockwise from the north position. At much lower Rayleigh numbers, vorticity is well distributed within the annulus, as shown in *Figure 3* for $Ra=1000$, $Pr=0.7$ and $r_2/r_1=2.6$ at the same angular locations as in *Figure 2*. At much higher Rayleigh numbers, vorticity approaches zero in most of the central portion of the annulus. This implies a stationary core region, and is similar to the natural convection flow in a vertical slot[28]. Results for streamlines and isotherms are available in the literature (e.g. Kuehn and Goldstein[1]), and are therefore not presented here.

On reading a recent paper of Himasekhar and Bau[12], who calculate natural convection in horizontal annuli containing saturated porous media, it occurred to us that we might, in our present problem, encounter bifurcation from the basic flow. We reasoned that for thin annuli

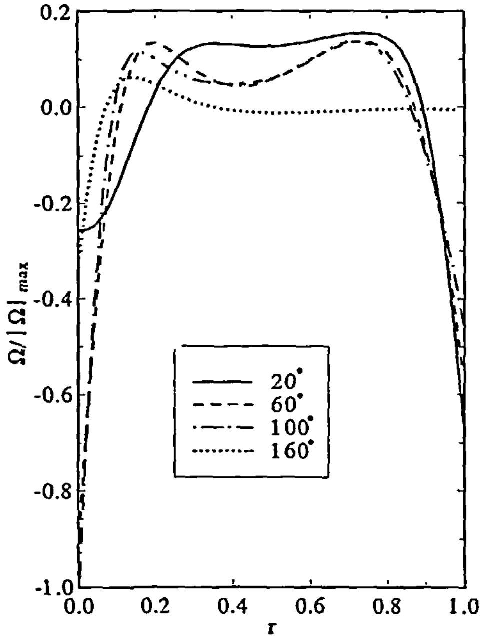

Figure 2 Vorticity distribution for $Ra = 50{,}000$, $Pr = 0.7$ and $r_2/r_1 = 2.6$ at various angular locations measured from the north position. $|\Omega|_{max} = 1192.2$.

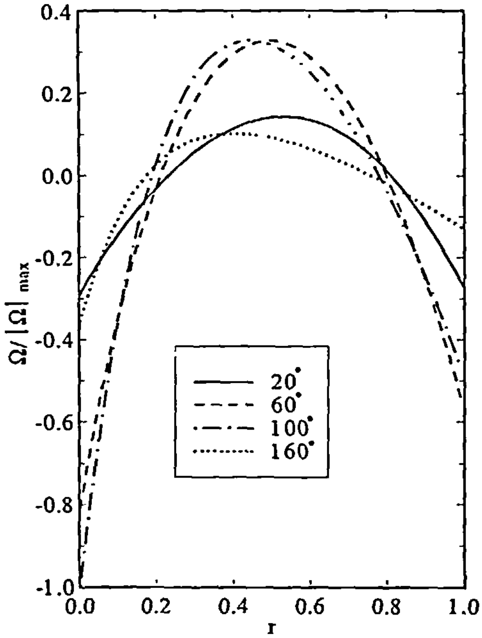

Figure 3 Vorticity distribution for $Ra = 1{,}000$, $Pr = 0.7$ and $r_2/r_1 = 2.6$ at various angular locations measured from the north position. $|\Omega|_{max} = 49.87$.

at either top or bottom locally the conditions correspond to those of the Benard problem and we investigated the existence of bifurcating solutions. Our conclusions are negative, however, as we found no bifurcation from the basic state up to 60,000 in the Grashof number. This finding is in stark contrast to the results obtained in saturated porous media.

In conclusion we may state that the Galerkin–spline formulation is a suitable strategy for cavity flow in natural convection problems, especially when streamfunction formulation is used. We find the accuracy of the Galerkin–spline formulation to be superior to the finite difference method for comparable size systems.

APPENDIX

Integration over the unit square R yields the Galerkin coefficients

$$\bar{Z}^{(\alpha)}_{ijk} = \int_0^1 b_i^{(a)}(\theta) b_j^{(b)}(\theta) b_k^{(c)}(\theta)\,\mathrm{d}\theta$$

$$\bar{z}^{(\alpha)}_{ij} = \int_0^1 b_i^{(b)}(\theta) b_j^{(c)}(\theta)\,\mathrm{d}\theta$$

$$\bar{b}_i^{(0)} = \int_0^1 b_i^{(0)}(\theta)\,\mathrm{d}\theta$$

$$\overline{bc}_i^{(0)} = \int_0^1 \cos(2\pi\theta) b_i^{(0)}(\theta)\,\mathrm{d}\theta$$

$$\overline{zc}_{ij}^{(\alpha)} = \int_0^1 \cos(2\pi\theta) b_i^{(b)}(\theta) b_j^{(c)}(\theta)\,\mathrm{d}\theta$$

$$\overline{zs}_{ij}^{(\alpha)} = \int_0^1 \sin(2\pi\theta) b_i^{(b)}(\theta) b_j^{(c)}(\theta)\,\mathrm{d}\theta$$

$$\overline{\mathrm{PK}}_{ijk}^{(\alpha)} = \int_0^1 X^K(r) A_i^{(a)}(r) A_j^{(b)}(r) A_k^{(c)}(r)\,\mathrm{d}r$$

$$\overline{\mathrm{pK}}_{ij}^{(\alpha)} = \int_0^1 X^K(r) A_i^{(b)}(r) A_j^{(c)}(r)\,\mathrm{d}r$$

$$\overline{\mathrm{NL}}_{ijk}^{(\alpha)} = \int_0^1 X^{-L}(r) A_i^{(a)}(r) A_j^{(b)}(r) A_k^{(c)}(r)\,\mathrm{d}r$$

$$\overline{\mathrm{nL}}_{ij}^{(\alpha)} = \int_0^1 X^{-L}(r) A_i^{(b)}(r) A_j^{(c)}(r)\,\mathrm{d}r$$

where $a \leqslant b \leqslant c$, $\alpha = a+b+c+2$ (if $a>0$)$+1$ (if $b>0$), $K \geqslant 0$, $L>0$, and superscripts a, b, and c imply the ath, bth and cth derivative of the spline.

ACKNOWLEDGEMENTS

A.Z.S. was partially supported by NSF under Grant No. MSM-8619048, during this project. Computing was made possible through a grant by the Pittsburgh Supercomputing Center for use of its CRAY Y-MP/832. Both of these supports are gratefully acknowledged.

REFERENCES

1 Kuehn, T. H. and Goldstein, R. J., *J. Fluid Mech.*, **74**, 695–719 (1976)
2 Charrier-Mojtabi, M. C., Mojtabi, A. and Caltagirone, J. P., *J. Heat Transfer*, **101**, 171–173 (1979)
3 Boyd, R. D., *Int. J. Heat Mass Transfer*, **24**, 1545–1548 (1981)
4 Date, A. W., *Int. J. Heat Mass Transfer*, **29**, 1457–1464 (1986)
5 Fusegi, T. and Farouk, B., *Proc. 8th Int. Heat Transfer Conf.*, **4**, 1575–1580 (1986)
6 Bubnovich, V. I. and Kolesnikov, P. M., *J. Eng. Phys.*, **51**, 1175–1181 (1986)
7 Kumar, R., *Int. J. Heat Mass Transfer*, **31**, 1137–1148 (1988)
8 Glakpe, E. K., Watkins, C. B., Jr. and Cannon, J. N., *Num. Heat Transfer*, **10**, 279–295 (1986)
9 Sun, R. and Zhang, X., *Proc. 8th Int. Heat Transfer Conf.*, **4**, 1569–1574 (1986)
10 Hessami, M. A., Pollard, A. and Rowe, R. D., *J. Heat Transfer*, **106**, 668–671 (1984)
11 Hessami, M. A., Pollard, A., Rowe, R. D. and Ruth, D. W., *J. Heat Transfer*, **107**, 603–610 (1985)
12 Himasekhar, K. and Bau, H. H., *J. Fluid Mech.*, **187**, 267–300 (1988)
13 Galdi, G. P. and Padula, M., *Arch Rat. Mech. Anal.*, **110**, 187–286 (1989)
14 de Boor, C., *A Practical Guide to Splines*, Springer-Verlag, Berlin (1978)
15 Ortega, J. M. and Rheinboldt, W. C., *Iterative Solution of Non-Linear Equations in Several Variables*, Academic Press, San Diego (1970)
16 Joseph, D. D., *Stability of Fluid Motions*, Springer-Verlag, Berlin (1976)
17 Keller, H. B., in *Applications of Bifurcation Theory* (Ed. P. Rabinowitz), Academic Press, San Diego (1977)
18 Szeri, A. Z., Schneider, S. J., Labbe, F. and Kaufman, H. N., *J. Fluid Mech.*, **134**, 103–131 (1983)
19 San Andres, A. and Szeri, A. Z., *J. Appl. Mech.*, **51**, 869–878 (1984)
20 Dai, R. X., Dong, Q. and Szeri, A. Z., *Int. J. Non-Linear Mech.* (in press) (1991)
21 Ji, Z. H., Rajagopal, K. R. and Szeri, A. Z., *J. Non-Newtonian Fluid Mech.*, **36**, 1–25 (1990)
22 Dai, R. X., Rajagopal, K. R. and Szeri, A. Z., *J. Non-Newtonian Fluid Mech.*, **38**, 289–312 (1991)
23 Szeri, A. Z., Giron, A., Schneider, S. J. and Kaufman, H. N., *J. Fluid Mech.*, **134**, 133–154 (1983)
24 Dai, R. X. and Szeri, A. Z., *Int. J. Non-Linear Mech.*, **25**, 45–60 (1990)
25 Singh, S. N. and Chen, J., *Num. Heat Transfer*, **3**, 441–459 (1980)
26 MacGregor, R. K. and Emery, A. F., *ASME Paper No. 68-HT-4* (1968)
27 Batchelor, G. K., *Q. Appl. Math.*, **12**, 209–233 (1954)
28 Rubel, A. and Landis, F., *Phys. Fluids* (*Suppl.*), **12** (II), 208–213 (1969)